JACS
JOURNAL OF THE AMERICAN CHEMICAL SOCIETY

Article

pubs.acs.org/JACS

Surface Interrogation Scanning Electrochemical Microscopy of $Ni_{1-x}Fe_xOOH$ ($0 < x < 0.27$) Oxygen Evolving Catalyst: Kinetics of the "fast" Iron Sites

Hyun S. Ahn and Allen J. Bard*

Center for Electrochemistry, Department of Chemistry, The University of Texas at Austin, Austin, Texas 78712, United States

Supporting Information

ABSTRACT: Nickel-iron mixed metal oxyhydroxides have attracted significant attention as an oxygen evolution reaction (OER) catalyst for solar fuel renewable energy applications. Here, we performed surface-selective and time-dependent redox titrations to directly measure the surface OER kinetics of Ni^{IV} and Fe^{IV} in NiOOH, FeOOH, and $Ni_{1-x}Fe_xOOH$ ($0 < x < 0.27$) electrodes. Most importantly, two types of surface sites exhibiting "fast" and "slow" kinetics were found, where the fraction of "fast" sites in $Ni_{1-x}Fe_xOOH$ matched the iron atom content in the film. This finding provides experimental support to the theory-proposed model of active sites in $Ni_{1-x}Fe_xOOH$. The OER rate constant of the "fast" site was 1.70 s^{-1} per atom.

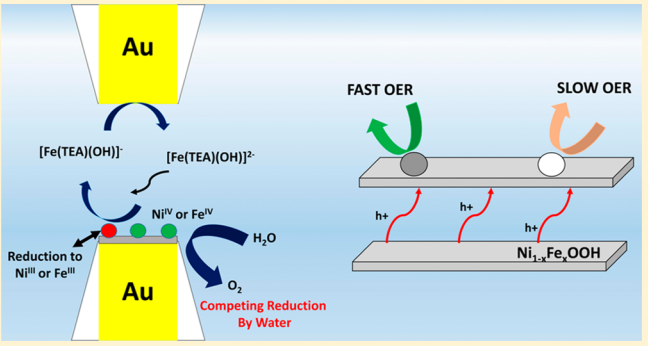

INTRODUCTION

The water oxidation half reaction has been studied widely in recent years due to its importance in the solar fuel generation process.[1,2] Its high thermodynamic barrier (1.23 eV) along with kinetic complexity involving four electrons and protons render it one bottleneck in achieving an overall solar to fuel pathway.[3] The development of an efficient and earth abundant catalyst for the oxygen evolution reaction (OER) is a key challenge for the renewable energy research community. In light of this, mixed metal oxides of nickel and iron have aroused much attention as a material exhibiting rapid catalysis at a moderate overpotential.[4−14] Recent composition activity analyses have revealed a range of optimum nickel-iron ratios for the best catalytic performance,[6,13−16] and a structural study by X-ray absorption spectroscopy (XAS) coupled with DFT suggested that isolated iron sites within a NiOOH matrix to be the active site.[17] Despite these advancements in the understanding of nickel-iron oxide OER, knowledge of the kinetics of the surface electron-transfer process is lacking. Also, the identity of the iron-active site proposed by a theoretical study needs to be further augmented experimentally.

We have recently reported on an application of a surface-specific electrochemical titration technique for a cobalt-based OER catalyst.[18] This variant of scanning electrochemical microscopy (SECM), surface interrogation (SI-SECM), quantitatively detects transient reactivity of surface species.[19] In this contribution, we analyze the surface chemistry of nickel, iron, and nickel-iron (up to 27% iron) oxyhydroxides by SI-SECM in an alkaline environment (2 M KOH). Surface active site densities in these oxyhydroxides were probed by redox titration at varying potentials (0.27−0.65 V). By time-dependent studies, with an improved resolution from our recent report (<10 ms),[20] the surface OER kinetics of nickel, iron, and nickel-iron were investigated. Importantly, our findings here revealed that in nickel-iron oxyhydroxides the number of reactive sites were proportional to the iron content in the electrode, which should serve as an experimental support to the theoretically proposed iron active site model.[17]

RESULTS AND DISCUSSION

SI-SECM Titration of NiOOH Surface. In a typical SI-SECM experiment, two size-matched ultramicroelectrodes (UMEs) are used at a close proximity such that the analyte generated by one electrode (tip or substrate) is quantitatively detected at the other electrode without leaving the tip−substrate gap.[19] In this study, two gold UMEs, substrate and tip, of radius a = 12.5 μm were used as shown in Scheme 1. The tip and substrate electrodes were aligned and approached to a distance of 2.0 μm, where quantitative detection of tip-generated analyte was achieved at the substrate (Scheme 1; for details on alignment and approach of the electrodes, see the Supporting Information). The catalyst films were deposited on the substrate electrode.[6,17] The redox mediator used in this work is a triethanolamine (TEA) complex of iron: $[Fe(C_6H_{12}NO_3)(OH)]^-$ ($FeTEA^{-/2-}$ E° = −1.05 V vs Ag/AgCl in 2 M NaOH).[21] According to the experimental diagram shown in Scheme 1, the redox mediator is in its oxidized state ($Fe^{III}TEA^-$) at the beginning of the experiment. At open circuit potential (OCP), the nickel atoms in the catalyst film are in their 2+ oxidation states.[17] As the substrate electrode is pulsed

Received: October 20, 2015
Published: December 8, 2015

DOI: 10.1021/jacs.5b10977
J. Am. Chem. Soc. 2016, 138, 313−318

Scheme 1. (A) Titration Sequence Scheme, (B) Series of Reactions Occurring at the Tip-Substrate Gap during Titration, and (C) Expected Titration CA Response in the Absence (black) and the Presence (red) of Surface Species That React with Tip-Generated Fe^{II} Titrant[a]

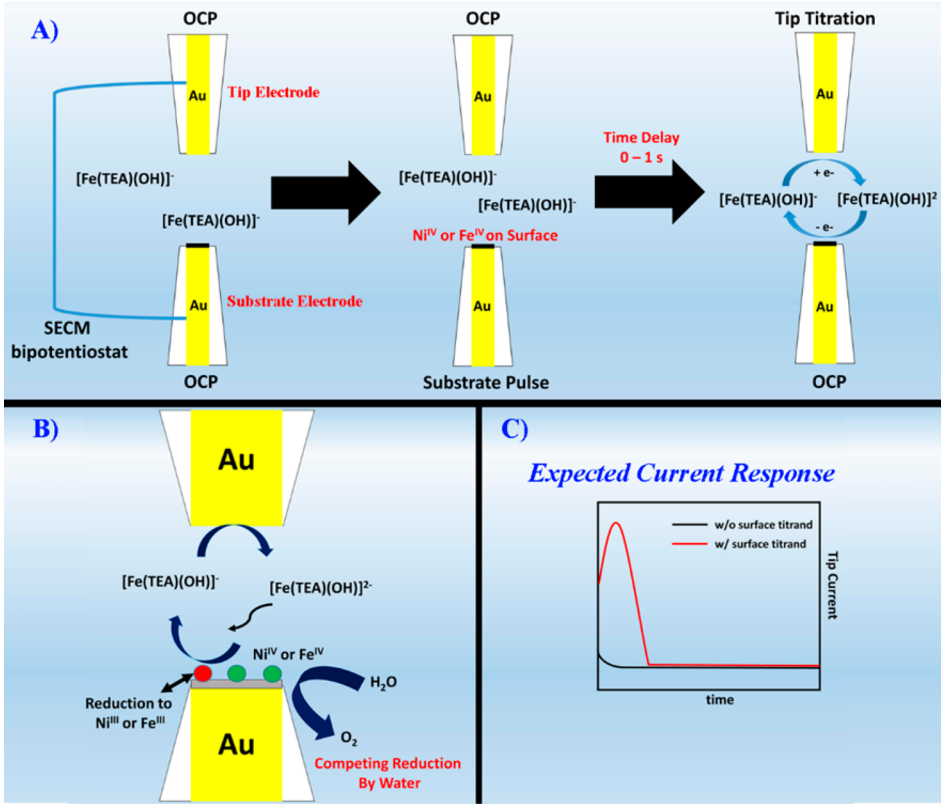

[a]Details: (A) titration sequence: resting at OCP (left), titrand generation by substrate pulse to E_{subs} (center), and titration by titrant generation at the tip electrode (right) and (B) tip generation of titrants, consumption of tirands (Ni^{III}, Ni^{IV}, and Fe^{IV}) by titrants, and OER by Ni^{IV} and Fe^{IV} in the absence of titrants.

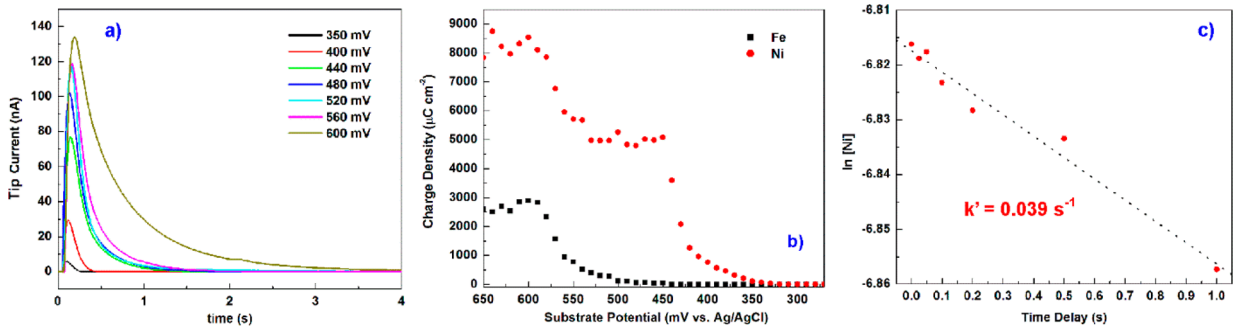

Figure 1. (a) Titration CA traces of $Ni(OH)_2$ at varying E_{subs} (inset label). Increased current level indicates the increased density of surface titrands formed at elevated E_{subs}. All CA traces shown are background subtracted and collected in 2 M KOH solution of 8 mM $[Fe(TEA)(OH)]^-$, as the tip was pulsed to −1.15 V. (b) Redox titration curves obtained from $Ni(OH)_2$ (red) and FeOOH (black) electrodes. Two transitions exhibited in the titration curve of $Ni(OH)_2$ are attributed to $Ni^{III/II}$ and $Ni^{IV/III}$, respectively. The sole oxidation in the titration of FeOOH is attributed to $Fe^{IV/III}$. In all of the titration curves, the margins of error were ca. 6% at E_{subs} < 0.5 V and 9−10% at E_{subs} > 0.5 V. Error bars were omitted for clarity. A plot including error bars can be found in Figure S10. (c) A time-dependent titration of $Ni(OH)_2$ (at E_{subs} = 0.6 V). Obtained titration charge densities are plotted against t_{delay}, and the loss in the obtained charge as a function of t_{delay} is due to Ni^{IV} OER in the absence of titrants (see also Figure S3).

to more positive potentials, the oxidation states of nickel atoms in the film reach 3+ or 4+, which has been seen by X-ray absorption spectroscopy.[17,22,23] The redox mediator is then reduced at the tip by application of a negative potential, introducing the titrant ($Fe^{II}TEA^{2-}$) that undergo reactions with Ni^{III} and Ni^{IV} reducing them back to Ni^{II} (Scheme 1B). The tip current decreases due to the reduction of $FeTEA^-$ measured by chronoamperometry (CA) back to the background level at negative feedback upon consumption of surface-active species (Scheme 1C). The pseudo-first-order reaction rate constants of Ni^{III} and Ni^{IV} with water can be determined by varying the time between active species production and tip generation of the titrant. The titration current should decay as a function of delay time (t_{delay}, the time between titrand formation and titrant generation) as water consumes Ni^{III} and Ni^{IV} in the absence of

DOI: 10.1021/jacs.5b10977
J. Am. Chem. Soc. 2016, 138, 313−318

the titrant. The potentials reported hereon are referenced to an Ag/AgCl (1 M Cl^-) electrode.

The oxidized surface titrands (Ni^{III} and Ni^{IV}) were generated by a potential pulse (0.27 to 0.65 V, 20 s in duration followed by open circuit) at the substrate electrode. The experimentally obtained titration CA traces are displayed in Figure 1a. As seen in each subsequent CA trace, more titrands were generated as a function of applied substrate potential (E_{subs}). The obtained titration amperograms were integrated to yield charge density—representative of the number of titrands per geometric electrode area—and plotted as a redox titration curve shown in Figure 1b. The plateau observed between E_{subs} of 0.45 and 0.55 V indicates the first hole equivalence of the surface, which is the $Ni^{III/II}$ transition. The subsequent rise in the charge density as a function of E_{subs} is attributed to the $Ni^{IV/III}$ transition. Higher than 3+ oxidation states by XAS were reported in a $Ni(OH)_2$ film as the electrode was poised at an oxidizing bias.[17,24] An overall nickel oxidation state of 3.4−3.6 was observed,[17,24] which is consistent with what we observed in this work (average nickel oxidation state of 3.6). An interesting feature to note from the $Ni(OH)_2$ titration curve in Figure 1b is the redox active site density. The density of redox sites in $Ni(OH)_2$ estimated from the $Ni^{III/II}$ plateau (ca. 5000 $\mu C \cdot cm^{-2}$) in the titration curve is 312 nickels per nm^2, much higher than that observed for a gold surface ({111}, 14 $Au \cdot nm^{-2}$, 225 $\mu C \cdot cm^{-2}$)[25] or that of a cobalt OER catalyst (17 $Co \cdot nm^{-2}$, 260 $\mu C \cdot nm^{-2}$; see Supporting Information for detailed calculations).[18,20] Such densely packed redox active sites cannot be easily comprehended by surface roughness and porosity alone. We postulate that the high density is due to charge transfer from the surface to the bulk material and perhaps some porosity of the film. We propose that (1) the layered structure of NiOOH allows partial access of the internals of the catalyst film and (2) hole conductivity across the layers of NiOOH is high such that it allows for the titration of the bulk of the film by oxidizing equivalence transfer to the solution−film interface. Catalyst films of FeOOH and $Ni_{1-x}Fe_xOOH$ also exhibit similar behavior (see below and Scheme 2).

Scheme 2. A Pictorial Representation of the Layered Structure of the Catalysts in Discussion, the Interlayer Hole Transfer Processes, and the Distinct "Fast" and "Slow" OER Catalytic Sites

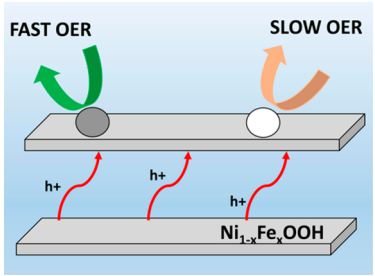

The OER kinetics of Ni^{III} and Ni^{IV} in NiOOH catalyst film was studied using a time-dependent titration method. A delay time t_{delay} was varied, in which the only decay mechanism of Ni^{III} and Ni^{IV} is via OER in the absence of other oxidizable species in solution. Obtained titration charge was then converted to ln [Ni] and plotted as a function of t_{delay} (Figures 1c and S3) to obtain the pseudo-first-order kinetic rate constant for OER (see Supporting Information for details). As seen in Figure S3 (at E_{subs} = 0.5 V), Ni^{III} was not potent enough to undergo OER, as evidenced by no time dependence in the titration current. The Ni^{IV} species in NiOOH exhibited a pseudo-first-order decay for OER (Figure 1c, at E_{subs} = 0.6 V) with a kinetic rate constant of 0.04 s^{-1}. This relatively slow rate constant is consistent with recent observations on macro electrodes of slow kinetics on nickel oxide surfaces.[8,9,17]

SI-SECM Titration of FeOOH Surface. A redox titration similar to that for $Ni(OH)_2$ described in the previous section was performed on a thin film of FeOOH. Amperograms obtained from titration experiments are shown in Figure S4, and the charge-integrated redox titration curve is exhibited in Figure 1b. Unlike in the case of nickel, only one oxidative transition ($Fe^{IV/III}$) was observed for FeOOH catalyst. This observation is consistent with those from XAS studies in the literature[17,21,22] as well as the cyclic voltammetry of FeOOH electrode (Figure S5). Earlier investigations have indicated that the film properties (thickness, porosity, and roughness) are similar between a film of FeOOH and that of $Ni(OH)_2$;[6,17] therefore the difference in the redox site density we find here (312 $Ni \cdot nm^{-2}$ and 185 $Fe \cdot nm^{-2}$, respectively) is attributed to the difference in the hole conductivity in the two films and the subsequent fractional participation of the bulk film in the FeOOH. Similar observation of limited conductivity in FeOOH films has been reported.[26]

The OER kinetics of Fe^{IV} was probed similarly to that performed for nickel, by variation of t_{delay} during titration. Log of the remaining surface Fe^{IV} concentration was plotted as a function of t_{delay} in Figure 2 (E_{subs} = 0.6 V). FeOOH revealed a marked different OER kinetic behavior, with a rapid quench of the "fast" active sites by water followed by a slow decay with a distinct rate constant (see also Figure S6). Pseudo-first-order OER rate constant of the "fast" iron sites was 0.18 s^{-1}, significantly faster than that of Ni^{IV}, whereas that of "slow" iron sites was similar to that of Ni^{IV} (Table 1). The two-time regions shown here in the ln [Fe] vs t_{delay} plot indicates that two distinct types of surface iron sites exist on an electrode poised at an oxidizing bias (enough for OER) exhibiting different chemistry with water. From our redox calculations presented here, the fraction of "fast" sites in our FeOOH film is ca. 8% of total irons, similar to the fraction of oxygen-deficient iron sites found in Fe_2O_3.[27]

SI-SECM Titration of $Ni_{1-x}Fe_xOOH$ (x = 0.09, 0.18, and 0.27) Surfaces. Similar to the cases with $Ni(OH)_2$ and FeOOH observed above, surface redox titration was performed on nickel-iron oxyhydroxide electrodes of composition containing 8.97, 18.19, and 27.31% iron, respectively (composition determined by energy dispersive X-ray spectroscopy). The obtained titration curves are presented in Figures 3a and S7. Most noticeably, in the nickel-iron mixed metal oxyhydroxides, the $Ni^{III/II}$, $Ni^{IV/III}$, and $Fe^{IV/III}$ transitions (simultaneous at ca. 0.45 V) occurred at negatively shifted potentials than those observed from $Ni(OH)_2$ and FeOOH. Because each of the three ($Ni^{III/II}$, $Ni^{IV/III}$, and $Fe^{IV/III}$) electron-transfer events is not resolved in E_{subs}, the surface active site density was not directly measurable. However, based on the similar catalyst film properties of $Ni_{1-x}Fe_xOOH$ and $Ni(OH)_2$[6,17] and treating the transition (at ca. 0.45 V) as an overall two-electron event, we can estimate that the surface active site density in the $Ni_{1-x}Fe_xOOH$ is similar to that in $Ni(OH)_2$. Concurrent to the cathodic shift of the metal oxidation potentials in the $Ni_{1-x}Fe_xOOH$, the OER potential was also negatively shifted, with active OER starting from E_{subs}

DOI: 10.1021/jacs.5b10977
J. Am. Chem. Soc. 2016, 138, 313−318

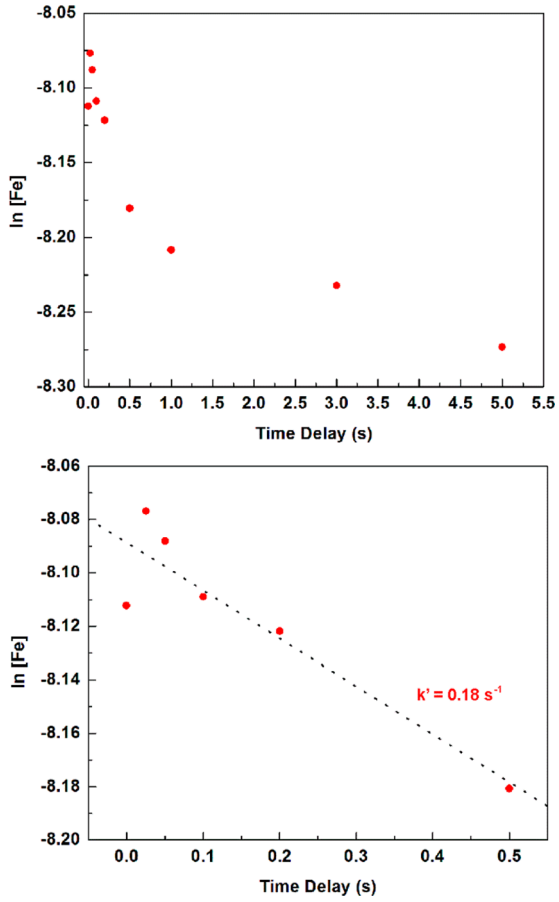

Figure 2. A time-dependent titration of FeOOH (top frame; at E_{subs} = 0.6 V). Obtained titration charge densities are plotted against t_{delay}, and the loss in the obtained charge as a function of t_{delay} is due to Fe^{IV} OER in the absence of titrants (see also Figure S6). Two time regions with distinct k' was observed. In the bottom frame, a time region with high k' ("fast" sites) is shown.

Table 1. Pseudo-First-Order OER Rate Constants of Various Catalysts Tested in This Work[a]

catalyst	Fe content (%)	"fast" site rate constant k' (s^{-1})	"slow" site rate constant k' (s^{-1})	"fast" site fraction (%)
NiOOH	<0.8	0.04 ± 0.03		
$Ni_{0.91}Fe_{0.09}OOH$	8.97	0.41 ± 0.03	0.01 ± 0.02	6.4
$Ni_{0.82}Fe_{0.18}OOH$	18.19	1.70 ± 0.07	0.04 ± 0.02	17.6
$Ni_{0.73}Fe_{0.27}OOH$	27.31	0.34 ± 0.17		
FeOOH	>98.3	0.18 ± 0.05	0.02 ± 0.02	8.6

[a]Noticeably, the "slow" sites in the nickel-iron materials all exhibited k' similar to that of Ni^{IV} in NiOOH. Also, the "fast" site fraction in the $Ni_{0.82}Fe_{0.18}OOH$ and $Ni_{0.91}Fe_{0.09}OOH$ electrodes agreed well with the iron atom content in the material.

of 0.45 V (see Figure S8; NiOOH and FeOOH OER at E_{subs} = 0.6 V). This lowering in the onset overpotential of ca. 0.15 V is also similar to that calculated from a DFT study.[17]

Time-dependent surface titration of the $Ni_{0.82}Fe_{0.18}OOH$ electrode is presented in Figure 3. Similar to that of the FeOOH electrode, two regions with distinct rate constants were observed (see Scheme 2). Quenching of the "fast" surface sites by water occurred within ca. 100 ms, followed by OER of the "slow" sites. The OER rate constant obtained for the "fast" sites in the $Ni_{0.82}Fe_{0.18}OOH$ electrode was 1.70 s^{-1}, much faster than those estimated from experiments on larger electrodes,[7−9,11,14] and similar to that of a Co^{IV} site that we measured via SI-SECM (1.2 s^{-1}).[18,20] The rate constant of the "slow" sites in the $Ni_{0.82}Fe_{0.18}OOH$ electrode is similar to that of Ni^{IV} in the NiOOH. Quite interestingly, the fraction of the "fast" sites in the $Ni_{0.82}Fe_{0.18}OOH$ catalyst film matches the iron content in the film very well (18.19% iron and 17.6% "fast" sites), suggesting that the dispersed iron sites in the NiOOH matrix is the identity of the "fast" site observed here. This also serves as the first experimental support for the theoretical model that suggested such active site structure.[17]

Redox titration was also performed on nickel-iron mixed metal oxyhydroxides of the compositions $Ni_{0.91}Fe_{0.09}OOH$ and $Ni_{0.73}Fe_{0.27}OOH$ (titration curves presented in Figure S7). In the case of $Ni_{0.91}Fe_{0.09}OOH$, the observed surface kinetic behavior was similar to that of $Ni_{0.82}Fe_{0.18}OOH$, exhibiting simultaneous access of $Ni^{III/II}$, $Ni^{IV/III}$, and $Fe^{IV/III}$ at E_{subs} = 0.45 V, and in the presence of "fast" and "slow" sites. The OER rate constants for "fast" and "slow" sites in $Ni_{0.91}Fe_{0.09}OOH$ were 0.41 and 0.01 s^{-1}, respectively. The "slow" site rate constant is similar to that of $Ni_{0.82}Fe_{0.18}OOH$; however, that of the "fast" site was 3-fold lower than that of $Ni_{0.82}Fe_{0.18}OOH$. This result is consistent with the activity of nickel-iron oxide films obtained from various composition analyses.[6,8,14] Optimum iron concentrations for best performance exist, and 10% is outside of the range. The "fast" site fraction agrees well with the iron content in $Ni_{0.91}Fe_{0.09}OOH$ (8.97% iron and 6.4% "fast" sites), though not as good of an agreement as that seen in $Ni_{0.82}Fe_{0.18}OOH$. The discrepancy in the k' of the "fast" sites between $Ni_{0.91}Fe_{0.09}OOH$ and $Ni_{0.82}Fe_{0.18}OOH$ may also be partially attributable to the lower "fast" site fraction compared to the iron content in the $Ni_{0.91}Fe_{0.09}OOH$ film. In the case of $Ni_{0.73}Fe_{0.27}OOH$, we have observed a titration curve similar to that of $Ni(OH)_2$ (Figure S7), suggesting that phase segregation of $Ni(OH)_2$ and FeOOH occurred. Preceding studies have reported that no phase segregation occurred at iron concentrations lower than 50%;[6,8] however, in our preparation on UMEs, phase segregation was always observed from samples with iron content >25%, similar to that found in more recent studies.[15,16] In the time-dependent study of $Ni_{0.73}Fe_{0.27}OOH$ catalyst, no clear sign of "fast" and "slow" active sites were observed (see Figure S9). However, a more enhanced OER rate constant (0.34 s^{-1}) compared to that of NiOOH was observed. With samples of >25% iron content the uncertainty in the k' measurement increased significantly (0.34 ± 0.17 s^{-1}), suggesting that reproducible preparation of the catalyst film was difficult due to an uncontrolled degree of phase segregation.

CONCLUSION

In this report we have performed surface selective redox titration of $Ni(OH)_2$, FeOOH, and $Ni_{1-x}Fe_xOOH$ electrodes. We observed unusually high densities of surface catalytic sites in these electrodes (ca. 300 atoms·nm^{-2}), suggesting that many atoms from the bulk (layers underneath the solution interface layer) are participating in the surface catalysis via fast interlayer hole transfer. Through time-dependent titrations we have shown that Ni^{IV} is indeed a poor OER catalyst as suggested by a theoretical study,[17] with a k' of 0.04 s^{-1} (see Table 1). Interestingly in FeOOH and $Ni_{1-x}Fe_xOOH$ electrodes (x < 0.25), we observed two types of catalytic sites exhibiting "fast" and "slow" OER behavior, respectively. The "fast" site fraction in the $Ni_{1-x}Fe_xOOH$ electrode coincided well with the iron

DOI: 10.1021/jacs.5b10977
J. Am. Chem. Soc. 2016, 138, 313−318

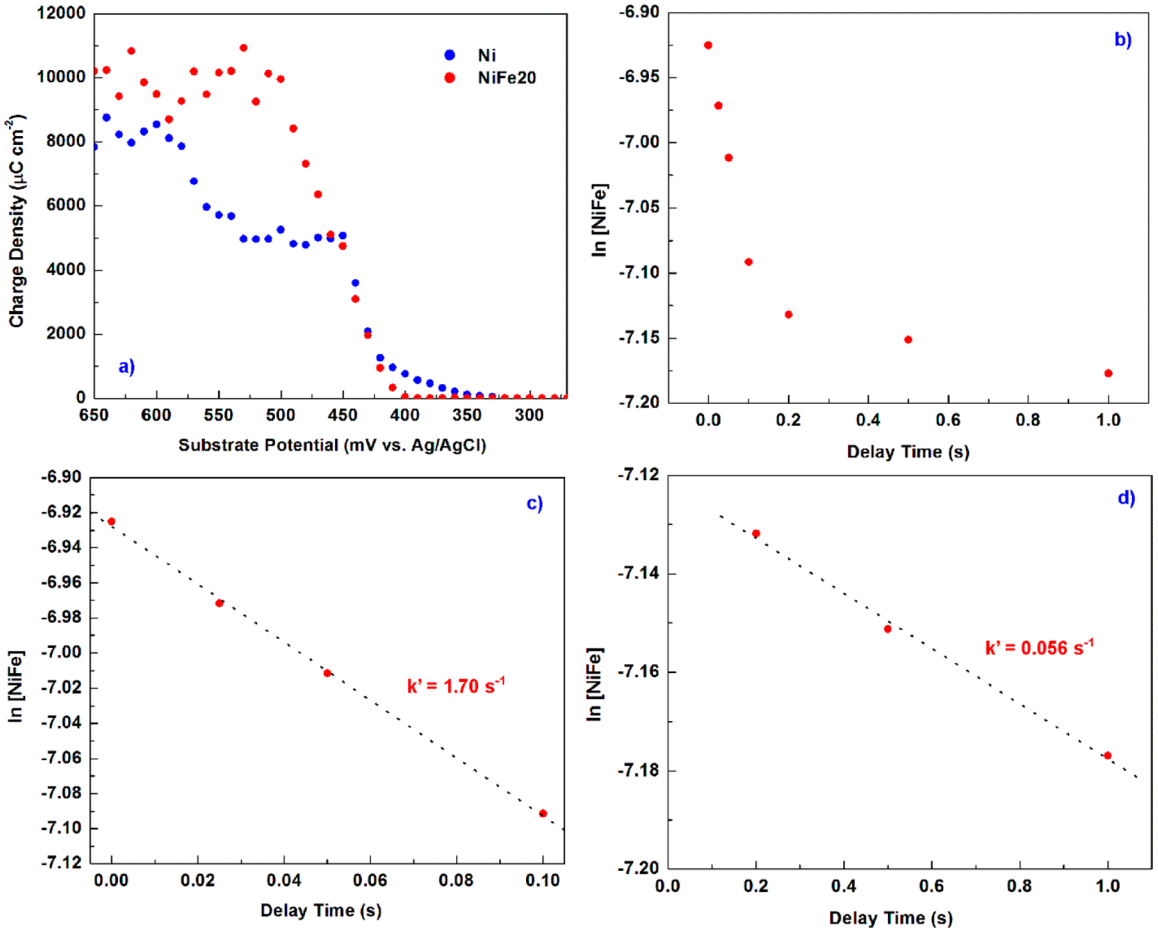

Figure 3. (a) A redox titration curve for $Ni_{0.82}Fe_{0.18}OOH$ is displayed alongside that of $Ni(OH)_2$. $Ni^{IV/III}$ and $Fe^{IV/III}$ transitions are noticeably cathodically shifted (ca. 0.15 V). (b) Time-dependent titration of the $Ni_{0.82}Fe_{0.18}OOH$ electrode is shown, exhibiting two time regions with distinct k', similar to that shown in the titration of FeOOH. (c) The OER rate constant of the "fast" sites in the $Ni_{0.82}Fe_{0.18}OOH$ electrode was determined by plotting ln [NiFe] as a function of t_{delay}, up to 100 ms. (d) ln [NiFe] as a function of t_{delay} in the "slow" site time region, displaying a similar rate constant to that of Ni^{IV}.

atom content in the film, suggesting that the identity of the "fast" active sites is indeed the dispersed iron atoms in a NiOOH matrix; one proposed by a DFT study but not previously shown experimentally.[17] Uncontrolled phase segregation into NiOOH and FeOOH was observed in $Ni_{1-x}Fe_xOOH$ electrodes when the iron content exceeded 25%. From this contribution we can conclude that the remarkable OER catalytic activity of the nickel-iron mixed metal oxyhydroxides arises from a combination of two effects: (1) high density of catalytically participating metal sites via fast hole conduction through the catalyst film (ca. 300 atoms·nm^{-2}, compared to those of Co_3O_4 and IrO_2, 17 nm^{-2} and 25 nm^{-2}, respectively)[18,20,28] and (2) fast OER kinetics on iron catalyst sites in NiOOH matrix with a rate constant of 1.70 s^{-1}.

EXPERIMENTAL SECTION

General. All solutions were prepared using Milli-Q deionized water (18.2 MΩ·cm, 4 ppb total oxidizable carbon). Triethanolamine (TEA, 99+%, Aldrich), $Fe(NO_3)_3·9\ H_2O$ (99+%, Acros), $FeSO_4·7\ H_2O$ (99.9%, Fisher), $NiSO_4·6\ H_2O$ (99.9+%, Alfa-Aesar), and sodium hydroxide (98.9+%, Fisher) were used as received. Gold wire (99.99+%) of 25 μm diameter was purchased from Goodfellow (Devon, PA). The gold wire was used to fabricate the SECM tips as described elsewhere.[29] All electrodes used in this study had an RG of ca. 1.3 and were polished with alumina paste on microcloth pads prior to use. The surfaces of the electrodes were cleaned with an acidic piranha solution (1:1 v/v 40% H_2O_2 and concentrated H_2SO_4) before the experiments. The $Ni(OH)_2$, FeOOH, and $Ni_{1-x}Fe_x(OH)_2$ OER catalyst films ($0 < x < 0.27$) were deposited onto a gold SECM tip (substrate electrode) by an electrophoretic deposition method described in the literature.[6,17] Briefly, the catalyst films were deposited electrophoretically from a solution containing 10 mM metal ions (combined 10 mM, Ni:Fe ratio varied for desired composition) by an application of a reducing bias at the working electrode. The cathodic current applied at the working electrode was 50 μA·cm^{-2}, for a duration of 25 s. For all electrochemical measurements an Ag/AgCl reference electrode and a platinum wire counter electrode were used. The $[Fe(TEA)(OH)]^-$ redox mediator (TEA = triethanolamine ($C_6H_{15}NO_3$), $E°$ = −1.05 V vs Ag/AgCl; see Supporting Information for details) was prepared as described in the literature.[21,28] The redox mediator solution was prepared freshly before each titration experiment and used for no more than 48 h.

Instrumentation. SECM experiments were conducted utilizing a CHI920C SECM station bipotentiostat and its built-in software (CH Instruments; Austin, TX). Chronoamperometry (CA) was chosen as a detection technique in the SI-SECM experiments. An external switching device controlling the two working electrodes of the SECM (tip and substrate) was implemented. For details of the setup, refer to refs 18, 20, and 28. The tip and the substrate electrodes (both 25 μm Au UME) were positioned at 2.0 μm from one another, a distance at which generation-collection efficiency was unity (refer to the Supporting Information for details of electrode alignment and placement). For each data point collected, the substrate was stepped to E_{Subs} for a time t_{step} = 20 s followed by a potential step back to open

DOI: 10.1021/jacs.5b10977
J. Am. Chem. Soc. 2016, 138, 313−318

circuit. A respective detection by stepping the potential of the tip was performed after a delay time t_{delay}. A total collection time of 15 s was selected for CA experiments. The redox mediator solutions employed in this work consisted of 8 mM [Fe(TEA) (OH)]$^-$ in 2 M KOH.

■ ASSOCIATED CONTENT

Supporting Information

The Supporting Information is available free of charge on the ACS Publications website at DOI: 10.1021/jacs.5b10977.

Electrode alignment and approach data, titration amperograms, CV of NiOOH, FeOOH, and $Fe_xNi_{1-x}OOH$ electrodes, and error analysis information (PDF)

■ AUTHOR INFORMATION

Corresponding Author

*ajbard@mail.utexas.edu

Notes

The authors declare no competing financial interest.

■ ACKNOWLEDGMENTS

This work was supported by NSF under the NSF Center CHE-1305124 and the Welch Foundation (F-0021).

■ REFERENCES

(1) Bard, A. J.; Fox, M. A. *Acc. Chem. Res.* **1995**, *28*, 141−145.
(2) Gray, H. B. *Nat. Chem.* **2009**, *1*, 7.
(3) Ahn, H. S.; Yano, J.; Tilley, T. D. *Energy Environ. Sci.* **2013**, *6*, 3080−3087.
(4) Corrigan, D. A. *J. Electrochem. Soc.* **1987**, *134*, 377−384.
(5) Guerrini, E.; Piozzini, M.; Castelli, A.; Trasatti, S. *J. Solid State Electrochem.* **2008**, *12*, 363−373.
(6) Louie, M. W.; Bell, A. T. *J. Am. Chem. Soc.* **2013**, *135*, 12329−12337.
(7) Hunter, B. M.; Blakemore, J. D.; Deimund, M.; Gray, H. B.; Winkler, J. R.; Müller, A. M. *J. Am. Chem. Soc.* **2014**, *136*, 13118−13121.
(8) Trotochaud, L.; Ranney, J. K.; Williams, K. N.; Boettcher, S. W. *J. Am. Chem. Soc.* **2012**, *134*, 17253−17261.
(9) Trotochaud, L.; Young, S. L.; Ranney, J. K.; Boettcher, S. W. *J. Am. Chem. Soc.* **2014**, *136*, 6744−6753.
(10) Li, Y.-F.; Selloni, A. *ACS Catal.* **2014**, *4*, 1148−1153.
(11) Gong, M.; Li, Y.; Wang, H.; Liang, Y.; Wu, J. Z.; Zhou, J.; Wang, J.; Reiger, T.; Wei, F.; Dai, H. *J. Am. Chem. Soc.* **2013**, *135*, 8452−8455.
(12) Młynarek, G.; Paszkiewicz, M.; Radniecka, A. *J. Appl. Electrochem.* **1984**, *14*, 145−149.
(13) Landon, J.; Demeter, E.; İnoğlu, N.; Keturakis, C.; Wachs, I. E.; Vasić, R.; Frenkel, A. I.; Kitchin, J. R. *ACS Catal.* **2012**, *2*, 1793−1801.
(14) Smith, R. D. L.; Prevot, M. S.; Fagan, R. D.; Trudel, S.; Berlinguette, C. P. *J. Am. Chem. Soc.* **2013**, *135*, 11580−11586.
(15) Klaus, S.; Cai, Y.; Louie, M. W.; Trotochaud, L.; Bell, A. T. *J. Phys. Chem. C* **2015**, *119*, 7243−7254.
(16) Swierk, J. R.; Klaus, S.; Trotochaud, L.; Bell, A. T.; Tilley, T. D. *J. Phys. Chem. C* **2015**, *119*, 19022−19029.
(17) Friebel, D.; Louie, M. W.; Bajdich, M.; Sanwald, K. E.; Cai, Y.; Wise, A. M.; Cheng, M.-J.; Sokaras, D.; Weng, T.-C.; Alonso-Mori, R.; Davis, R. C.; Bargar, J. R.; Nørskov, J. K.; Nilsson, A.; Bell, A. T. *J. Am. Chem. Soc.* **2015**, *137*, 1305−1313.
(18) Ahn, H. S.; Bard, A. J. *J. Am. Chem. Soc.* **2015**, *137*, 612−615.
(19) Rodríguez-López, J.; Alpuche-Avilés, M. A.; Bard, A. J. *J. Am. Chem. Soc.* **2008**, *130*, 16985−16995.
(20) Ahn, H. S.; Bard, A. J. *Anal. Chem.* **2015**, *87*, 12276−12280.
(21) Bechtold, T.; Burtscher, E.; Gmeiner, D.; Bobleter, O. *J. Electroanal. Chem. Interfacial Electrochem.* **1991**, *306*, 169−178.
(22) Gajda-Schrantz, K.; Tymen, S.; Boudoire, F.; Toth, R.; Bora, D. K.; Calvet, W.; Grätzel, M.; Constable, E. C.; Braun, A. *Phys. Chem. Chem. Phys.* **2013**, *15*, 1443−1451.
(23) Axmann, P.; Glemser, O. J. *J. Alloys Compd.* **1997**, *246*, 232−241.
(24) Bediako, D. K.; Lassalle-Kaiser, B.; Surendranath, Y.; Yano, J.; Yachandra, V. K.; Nocera, D. G. *J. Am. Chem. Soc.* **2012**, *134*, 6801−6809.
(25) Herrero, E.; Buller, L. J.; Abruña, H. D. *Chem. Rev.* **2001**, *101*, 1897−1930.
(26) Burke, M. S.; Kast, M. G.; Trotochaud, L.; Smith, A. M.; Boettcher, S. W. *J. Am. Chem. Soc.* **2015**, *137*, 3638−3648.
(27) Fu, Q.; Li, W.-X.; Yao, Y.; Liu, H.; Su, H.-Y.; Ma, D.; Gu, X.-K.; Chen, L.; Wang, Z.; Zhang, H.; Wang, B.; Bao, X. *Science* **2010**, *328*, 1141−1144.
(28) Arroyo-Curras, N.; Bard, A. J. *J. Phys. Chem. C* **2015**, *119*, 8147−8154.
(29) Bard, A. J.; Mirkin, M. V. *Scanning Electrochemical Microscopy*, 2nd ed.; CRC Press: Boca Raton, FL, 2012.

DOI: 10.1021/jacs.5b10977
J. Am. Chem. Soc. 2016, 138, 313−318